Enhanced Performance for SSB-OFDM Transmission with a Low-Chirp Silicon MRM

Zibo Zheng, Xun Guan, *Member, IEEE*, Alireza Geravand, *Student Member, IEEE, Optica*, Wei Shi, *Senior Member, IEEE, Optica*, and Leslie A. Rusch, *Fellow, IEEE*, *Fellow, Optica*

***Abstract*—While single sideband (SSB) modulation with orthogonal frequency-division multiplexing (OFDM) is used to avoid chromatic dispersion (CD)-induced fading, it is only effective in the absence of chirp. We examine the effectiveness of a extremely wideband silicon photonics (SiP) microring modulator (MRM) modulator designed for low chirp operation. We identify and confirm via simulation and experiment two independent sources of signal impairment from MRM chirp. Signal throughput can be as much as doubled when using a low-chirp design. This enables adoption of very small, low power, easily integrated SiP modulators for short-reach applications at very high throughput.**

***Index Terms*—Silicon micro-ring, chirp, chromatic dispersion, direct detection, single-side band.**

I. Introduction

SILICON modulators are excellent candidates for access networks, such as radio access networks (RANs) and passive optical networks (PONs) [1]. Among various types of silicon modulators, silicon MRMs are particularly attractive due to their ultra small footprint, low power consumption, and compatibility with complementary metal-oxide-semiconductor (CMOS) technology [2].

We examine the application of SiP MRM modulators with direct detection for OFDM, contrasting with previous works focusing on pulse amplitude modulation. We use a new SiP MRM designed for wide bandwidth and low chirp. For the first time, we demonstrate and quantify experimentally the advantages of an IQ MRM with four rings (low chirp) vis-à-vis the two-ring solution in the presence of dispersion. In our demonstrations we succeed in isolating two independent sources of degradation: chirp-induced residual sideband and chirp-enhanced signal-to-signal beat interference (SSBI).

Direct detection OFDM offers tolerance to CD and polarization mode dispersion (PMD) in fiber transmission [3]. As double sideband (DSB)-OFDM suffers from power fading due to CD [4], [5], we focus on SSB-OFDM as in [6], [7]. There have been demonstrations of SSB-OFDM generation by silicon IQ Mach-Zehnder modulator (MZM) [8] and silicon IQ MRM [9], [10].

Frequency chirp can distort the optically modulated signal [11]. The push-pull method has been used to eliminate frequency chirp of $LiNbO_3$ MZMs by modulating two complementary signals onto the two MZM arms, which are π phase shifted [12]. This method has also been applied to silicon MZM [13]. For double sideband (DSB) PAM transmission, negative chirp in SiP MRM was embraced to dampen the effect of CD-induced fading in simulation [14] and experiments [15] [16]. However, regardless of its sign, chirp has a serious negative impact on SSB-OFDM signaling. There are a few reports on the impact of MRM chirp on transmission performance of optical SSB signal, for instance in [17].

Spectrally and power efficient SSB-OFDM (with guard bands smaller than the signal band, and reasonable carrier power), suffer from SSBI with direct detection. This effect has been investigated and mitigated with various compromises on guard band and high carrier-to-signal power ratio (CSPR), as in [18]. The study in [19], with an example where chirp originated in the directly modulated laser (DML), found that chirp, regardless of its sign, would further deteriorate SSBI and degrade OFDM performance. This can be combated by the added complexity and power consumption of nonlinear Volterra equalization, as in [20].

To avoid signal deterioration with chirp in a SiP MRM, a push-pull structure was used in [21], [22]. We designed a high-bandwidth MRM with low chirp, with a push-pull dual-arm drive for IQ modulation. We demonstrated Tb/s transmission with coherent detection using this extremely wideband IQ modulator to generate amplitude phase shift keying (APSK) [23] and quadrature amplitude modulation (QAM) [24], [25]. Here we explore direct detection with the same modulator.

In this paper, we isolate two sources of signal degradation due to chirp. In section II, we use a simple chirp model to simulate signal degradation. We show that residual sidebands result when there is imbalanced, non-zero chirp in the IQ arms. Experiments confirm this prediction. We describe via simulation how chirp will also lead to increased SSBI. In section IV we concentrate on residual sideband effects and quantify experimentally the advantage of our 4R push-pull modulator. In section V, we turn to the effect of chirp on SSBI, and again quantify the advantage of a low-chirp solution. In section VI we offer some discussion on our results, and we conclude the paper in section VII.

II. MRM Operation and Experimental Setup

We designed a wideband microring modulator (MRM) for complex IQ modulation, with a push-pull configuration in each

The work is partially supported by the Canada Natural Science and Engineering Council under the Discovery Grant program.

Z. Zheng, A. Geravand, L. A. Rusch, and W. Shi are with Centre for Optics, Photonics and Laser, Université Laval, Québec, Canada.

X. Guan, corresponding author, is with Tsinghua Shenzhen International Graduate School, Tsinghua University, Shenzhen, China; and also with Centre for Optics, Photonics and Laser, Université Laval, Québec, Canada.

arm for low-chirp operation [24]. In this paper, we show the importance of the low-chirp characteristics of this SiP solution when using the IQ structure to generate single sideband (SSB) OFDM.

A. MRM design

The MRMs were fabricated on a 220-nm-thick silicon-on-insulator platform. Each MRM has an add-drop racetrack shape with a 10 μm radius, 600 nm coupler length, and a 200 nm coupler gap. The MRMs are designed in the over-coupling regime for a smooth π phase shift across the resonance, to facilitate low-chirp with push-pull operation. The through ports are used for signal propagation.

Our IQ modulator has four MRMs arrayed on the chip as illustrated in Fig. 1a. Each branch (I and Q) has two rings in a push-pull configuration for low chirp. We characterized the fabricated chip used in the experiments which had a 59 GHz bandwidth, an extinction ratio of 20 dB, and a free-spectral range of 9.73 nm for each ring. The measured optical loss of the PN-junction-loaded waveguide phase shifter is 68 dB/cm. The total on-chip optical insertion loss is approximately 13 dB. Each MRM has efficiency $V_\pi L$ around 0.96 V·cm at 0.5 V reverse bias, i.e., a V_π of about 15 V. More details on the fabricated chip can be found in [23].

The MRM resonance wavelength is controlled by on-chip micro-heaters. We monitor optical power on the drop port of rings with on-chip Ge-on-silicon photodetectors. The photodetected control signals are connected to off-chip logarithmic transimpedance amplifiers in a feedback loop [23].

B. SiP MRM for SSB

We included several heaters on the fabricated chip for tuning phase, detuning on wavelength and tuning splitting ratio combined with Mach-Zehnder interferometer (MZI). In particular, we will use this flexibility to examine a four-ring low-chirp and a two-ring chirped configuration. As seen in Fig. 1b, for the two-ring chirped configuration we send all power to the upper branch; the lower branch is idle. We are essentially repurposing the push-pull branching into an IQ modulator. The figures note the phase shifts set by tuning.

Consider the transmission spectra of the I (or Q) branch of the two-ring (2R) configuration, as sketched to the right in Fig. 1b. We detune the two MRMs to operate at quadrature on the blue side of the resonance (leading to negative chirp). This places the laser center wavelength on the mutual operating point of the two rings. As the RF signal swings, the transmission response shifts and the signal experiences the inherent chirp of the MRM.

For the four-ring (4R) configuration, we operate in push-pull in the I (or Q) branch: data (push) and data-bar (pull) are routed to the rings. The transmission spectra of the four rings are given to the right in Fig. 1a. The static response of the push-pull rings are set to have detuning symmetric about the laser wavelength. In this way the chirp in each arm is canceled by the other arm, leading to low-chirp.

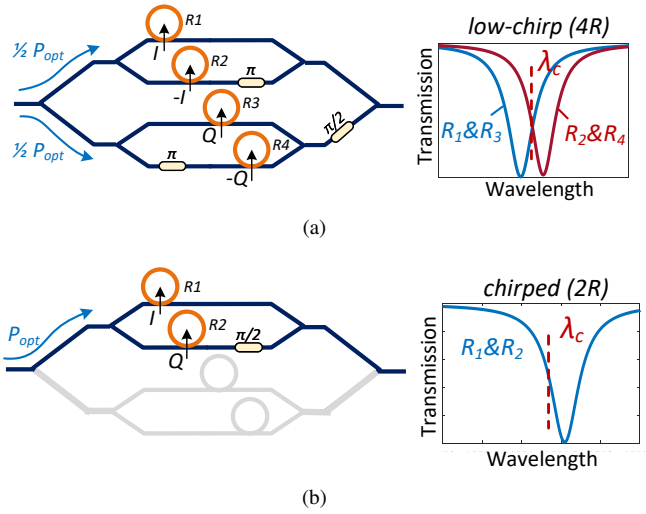

Fig. 1. Sketch of MRM structure and transmission spectrum for a) 4R (low-chirp) SSB-OFDM structure, and b) 2R (chirped) test configuration.

C. Experimental setup

The experimental setup is shown in Fig. 2. The source external cavity laser (ECL) is amplified by a high-power erbium doped fiber amplifier (EDFA) to create an optical carrier with center wavelength around 1550.3 nm and 23 dBm power. We use the high optical power to compensate for coupling loss in optical packaging, which is about 14 dB from on-chip back-to-back (B2B) measurement.

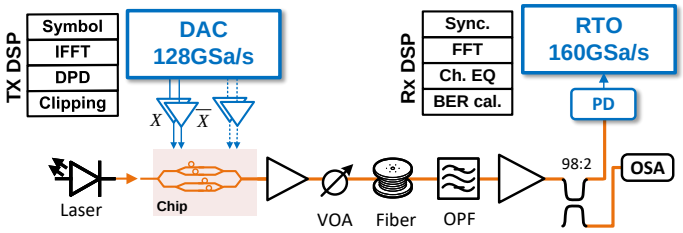

Fig. 2. Transmission setup with TX/RX DSP stack.

The MRM output is boosted by an EDFA and we adjust a variable optical attenuator (VOA) to keep power at 2 dBm when launching into fiber. After fiber transmission, we amplify with a second EDFA to compensate fiber attenuation. We use a 98:2 coupler to monitor the optical spectrum via a high resolution optical spectrum analyzer (OSA) from the two percentage port. As we do not have a transimpedance amplifier (TIA) embedded in or after photodiode (PD), we target received optical power of 6 dBm to ensure good signa-to-noise ratio (SNR).

We use an optical filter (Finisar Waveshaper 4000S) after the fiber as a flat band-pass filter with 1.5 nm width, to remove out-of-band amplified spontaneous emission (ASE) noise. We can also program the filter to suppress residual sideband by shifting the center wavelength and reducing the passband to 0.86 nm, in order to suppress lower side-band power, to verify enhanced SSBI impact, see Section V.

At the transmitter side, we generate QAM symbols for 2048 subcarriers. We pass this data through inverse fast Fourier

This article has been accepted for publication in IEEE/OSA Journal of Lightwave Technology. This is the author's version which has not been fully edited and content may change prior to final publication. Citation information: DOI 10.1109/JLT.2024.3362248

transform (IFFT) in the digital domain to produce a complex time domain signal. We apply a digital pre-distortion (DPD) filter to this signal to compensate the bandwidth roll-off of the digital-to-analog converter (DAC) and other RF components. We clip the real and imaginary parts of pre-compensated signal separately to around 9 dB peak-to-average power ratio (PAPR). We use high-speed DAC channels (Micram DAC5, 128 GSa/s) to generate RF signals up to 60 GHz. We use an RF amplifier (60GHz, SHF S804B) to boost the power, and an RF phase shifter to adjust the time delay between signal tributaries. At the receiver side, we first synchronize the signal frame and then perform fast Fourier transform (FFT) to recover the modulated symbols. We estimate the channel response by using a 16-symbol training sequence. we then apply the inverted channel to the remaining 200+ OFDM symbols, for a training overhead less than 10%. We estimate the SNR of each subcarrier, and count errors to estimate bit error rate (BER).

III. Impact of Chirp on SSB-OFDM

We observe two effects of transmitter chirp that worsen SSB-OFDM performance: 1) chirp induces a residual sideband that causes fading at the receiver side, and 2) chirp enhances the SSBI. We examine our SSB-OFDM spectra experimentally, and introduce a simple mathematical model for chirp. We use our model to describe the source of the two types of impairments.

A. Experimental SSB-OFDM Spectra

We test SSB-OFDM with two bandwidth allocations. One allocation has an 8 GHz guard band and a 32 GHz single-sideband signal. The other allocation has a 12 GHz guard band and a 48 GHz single-sideband signal, i.e., covering a 50% wider band. These choices allow us to investigate the severity of chirp-induced impair in the presence of chromatic dispersion, as we move to higher data rates enabled by the increased bandwidth of the latest SiP MRMs. The push to higher throughput and bandwidth stresses the importance of low-chirp architectures.

Figure 3 shows the experimental spectrum of each frequency allocation. We present the optical spectrum from both chirped (2R) and low-chirp (4R) modulators. We measured the CSPR to be between 9 to 10 dB for all cases. We calculate the OSNR (0.1 nm resolution) for a signal bandwidth of 32 GHz, to be roughly 17.3 dB (2R) and 17.7 dB (4R). For 48GHz, the OSNR is around 13.6 dB (2R) and 14.1 dB (4R). We see the spectra produced from 2R and 4R modulators overlap and have very similar optical signal-to-noise ratio (OSNR) in the main signal band. Therefore, the OSNR for both architectures is not the source of different behavior, but rather the performance discrepancy will be attributable to SNR differences.

B. Chirp model for spectral effects

We investigate MRM chirp via numerical modeling to see the impact on SSB signaling and transmission. In Fig. 4a we plot in a thick black line the intensity (transmission) response of a generic MRM. The phase response of an ideal, chirp-free modulator is given in a thin blue line. For SSB-OFDM

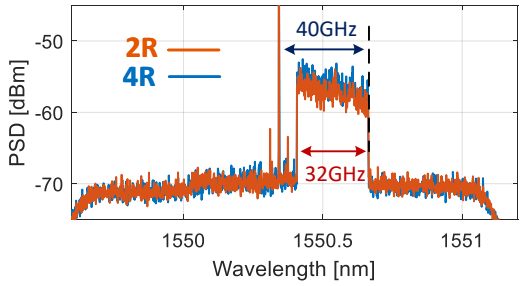

(a)

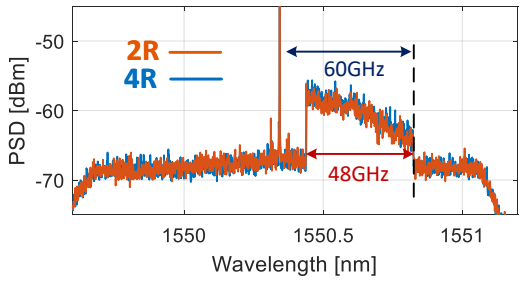

(b)

Fig. 3. Measured OFDM power spectral density for two testing scenarios: (a) 8 GHz guard band, 32 GHz signal band; (b) 12 GHz guard band, 48 GHz signal band.

with intensity modulation we bias at quadrature; see dot on transmission response in Fig. 4a. During RF modulation the transmission response moves right and left. The maximum RF swing is restricted to not exceed the resonance point (i.e., the null point, the lowest point in the transmission curve). We neglect the asymmetric shape of a true power transfer function to focus on chirp.

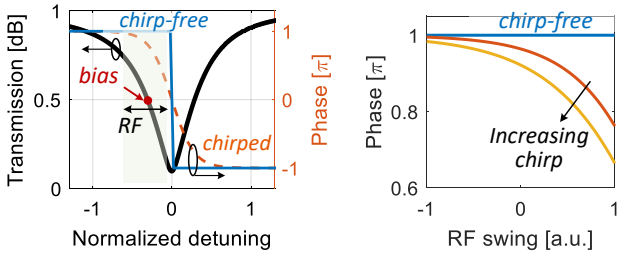

(a) (b)

Fig. 4. Simulation model of chirp. Left: extracted power transfer function and phase response by detuning. Right: simulated phase response associated with input RF swing by quad point biasing.

Let the applied voltage waveform be $s(t)$. We call $\phi(t)$ the chirp of the modulator, which introduces a time dependence to the frequency. The modulator output of a single ring in the presence of chirp is [12]

$$E_{out}(t) = E_s(t) \cdot e^{-j\phi(t)} \tag{1}$$

where $E_s(t)$ is the amplitude of the modulated optical signal produced by the driving electrical signal $s(t)$. The temporal behavior of the chirp is determined by $s(t)$. A chirp-free modulator would have constant ϕ instead of time-varying phase.

We use the hyperbolic tangent function to model $\phi(t)$, with α parameterizing the severity of the chirp, i.e.,

$$\phi(t) = -\pi \cdot \frac{e^{\alpha s(t)} - e^{-\alpha s(t)}}{e^{\alpha s(t)} + e^{-\alpha s(t)}} \tag{2}$$

Using this model and $\alpha = 1$ we produce the chirped phase response (right y-axis) in the thin dotted orange line in Fig. 4a. The transmission curve (i.e., intensity, left y-axis) is given in a thick line. A chirp-free phase response is given in the thinner solid line and is a step function. We extracted amplitude and phase responses over the detuning; our normalization defines detuning of one as the detuning produced by 1V on the controlling heater.

In Fig. 4b we sweep the RF swing and record the phase at the RF peak voltage. We ensure that our RF peak voltage never pushes us beyond the null point. Chirp-free ($\alpha = 0$) operation has phase in the flat, horizontal region. The phase is constant whether the RF voltage is positive or negative, as seen in the figure. For non-zero α the RF swing falls in the sloped section of the tanh. This leads to phase variation with RF swing. We see in Fig. 4b that as chirp increases, the phase response becomes non-constant, and also asymmetric with positive and negative driving voltage. The chirp leads to more severe signal distortion for larger α.

For a non-push-pull configuration, the 2R modulator producing SSB-OFDM would have output intensity

$$E_{SSB}(t) = E_I(t)e^{-j\phi_I(t)} + j \cdot E_Q(t)e^{-j\phi_Q(t)} \tag{3}$$

where $E_I(t)$ is the amplitude of modulated optical signal and $\phi_I(t)$ is the chirp produced phase function in the in-phase (I) branch. We ignore the common phase and carrier frequency term in Eq. 3. Similar definitions apply to the quadrature (Q) branch. The response in each branch is the response of a single ring.

For a push-pull configuration with a 4R modulator the intensity produced in the I branch is due to two rings modulated with inverse signals, i.e.,

$$\begin{aligned} &\frac{1}{2}\left\{E_I(t)e^{-j\phi_I(t)} + E_I(t)e^{j(\phi_I(t)+\pi)}\right\} \\ &= E_I(t)\cos\left(\phi_I(t) + \frac{\pi}{2}\right) \cdot e^{j\frac{\pi}{2}} \end{aligned} \tag{4}$$

We see that function $\phi(t)$ is no longer a chirp - it no longer affects frequency, which is now constant. This function does affect the amplitude, due to phase-amplitude modulation by the MZI structure for our two rings (in the I branch). The same reasoning applies to the Q branch. The push-pull function also renders the power transfer function more linear [26]. In practice, a 4R push-pull modulator will have some non-ideal structures leaving residual chirp, so we refer to the 4R as having low chirp.

C. Chirp-induced residual sideband

To avoid fading, we turn to SSB signaling. In experiments with our MRM, however, we see evidence of fading nonetheless in our 48 and 60 GHz SSB-OFDM experiments. We were able to compensate all imbalance between I and Q branches using on-chip heaters, so we know this is not the source of a residual sideband (see appendix . We suspect a chirp-related residual sideband is present, but could not discern such a sideband given the OSA noise floor.

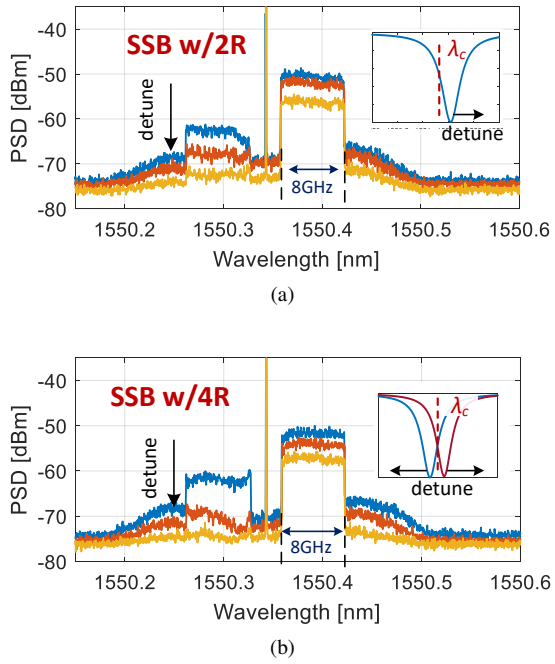

Fig. 5. Measured spectra showing residual sidebands at different detunings for a) 2R and b) 4R modulators; detuning process illustrated in insets.

We manipulated our test setup to help us visualize sideband suppression. We examined a small OFDM bandwidth (2 GHz guard band, 8 GHz signal bandwidth) to enhance RF power. This kept the signal well above the OSA noise floor. We purposely detuned the modulators to create a large residual sideband. We progressively reduce the detuning, and observe the dwindling sideband. We plot our measured spectra for the 2R modulator in Fig. 5a and the 4R modulator in Fig. 5b. The insets show how the detuning is applied in each case. We found the optimal detuning with lowest residual sideband. We can see that the lower chirp 4R modulator has a residual sideband smaller than that of the chirped 2R modulator.

We turn to our model to explain this observed behavior. We simulate SSB-OFDM spectra for a 2R modulator in three scenarios. The first scenario has no chirp. The second scenario has the same level of chirp on each ring. The third scenario has similar but unequal chirp on each ring. We plot our simulation results in Fig. 6. The chirp-free spectra is the classic SSB-OFDM with rectangular specturm and zero sideband. We plot the spectrum for equal chirp $\alpha = 1$ in each arm in Fig. 6a. The chirp introduces significant out-of-band power, but no discernible residual sideband. We plot the spectrum for slightly offset chirp (α =.9 and 1.1)in each arm in Fig. 6b. Again there is out-of-band power, and now we have a visible sideband.

Chromatic dispersion-induced fading will occur when any signal energy is in the negative frequency band. Even with identical chirp in I and Q branches, the leakage of signal energy from the desired band will lead to fading. Given fabrication uncertainty, slightly different chirp is not unexpected. Our simulations follow the trend seen in measurements

This article has been accepted for publication in IEEE/OSA Journal of Lightwave Technology. This is the author's version which has not been fully edited and content may change prior to final publication. Citation information: DOI 10.1109/JLT.2024.3362248

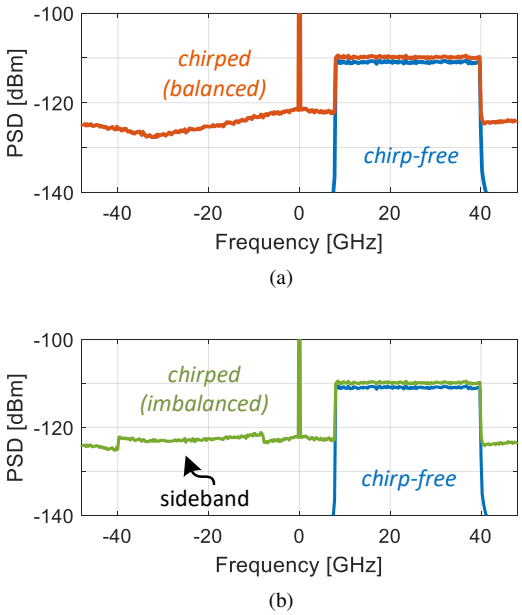

Fig. 6. Simulated spectra of SSB-OFDM produced by a 2R modulator with a) equal levels of chirp in each arm, and b) unequal levels of chirp; a simulated chirp-free spectra is provided for reference.

reported in Fig. 5 and reinforce our interpretation of the fading resulting from chirp-induced residual sideband.

D. Chirp-enhanced SSBI

We will see in later sections that even when filtering the out-of-band signal energy, we saw improved performance with a 4R modulator. In such a scenario, there can be no fading. We therefore turn to simulation to find the source of degradation in the presence of chirp but no fading.

With direct detection, the carrier beats with the OFDM signal band to produce the received signal

$$|C + E_s(t)|^2 = C^2 + C \cdot \left(E_s(t) + E_s^*(t)\right) + |E_s(t)|^2. \quad (5)$$

where C is the carrier power, and $E_s(t)$ is the optical SSB-OFDM signal. The second term is the desired OFDM signal, while the last term $|E_s(t)|^2$ is signal-to-signal beat interference (SSBI). A guard band is used to avoid the brunt of the SSBI, but to preserve spectral efficiency some SSBI is tolerated.

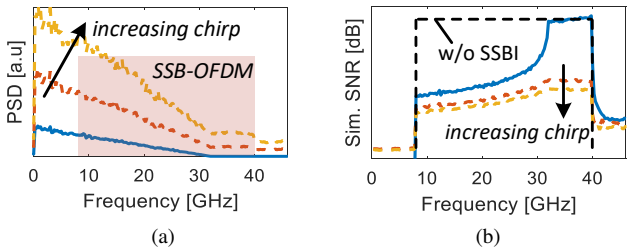

Fig. 7. Simulation for α=0, 1 and 1.5 of a) SSBI triangular spectra, and b) resulting SNR for the OFDM signal.

Using the chirp model in (2), we simulated the SSB-OFDM signal with 8 GHz guard band and 32 GHz passband. The rectangular in Fig. 7 represents the desired OFDM spectrum. The triangular spectra of the SSBI for α = 0, 1 and 1.5 are plotted in linear scale in Fig. 7. For chirp-free operation, the overlap of the triangular SSBI and rectangular OFDM spectra is tolerable. However, for increasing chirp we can see the SSBI power is enhanced and performance will suffer.

To quantify the performance degradation, we simulate the SNR in the OFDM signal band. We plot SNR in Fig. 7b with chirp-free as a solid line, and chirp versions dashed. The signal degradation for the chirp-free case is the trade-off used for a small guard band. This spectral region has SNR that is not much worsened by chirp. However, there is significant SNR degradation at higher frequencies, frequencies which were untouched by SSBI in the zero-chirp case. We will validate this enhancement experimentally in Section V.

IV. Low-Chirp Improvement vis-à-vis Residual Sideband

We quantify experimentally the performance improvement when using a 4R modulator. We confirm that both 2R and 4R experience performance degradation consistent with fading effects despite SSB operation. We present relative performance for various levels of accumulated dispersion.

A. Experimental confirmation of chirp-induced residual SSB

To confirm that performance is impacted by fading due to the presence of a residual sideband, we examine various levels of accumulated dispersion for the SSB-OFDM transmission. For each experiment we plot a theoretical fading curve for a given accumulated dispersion DL, where D is the dispersion coefficient of the fiber and L is the length. Details of our calculation of the fading response are provided in the appendix.

The OFDM performance is determined by subcarrier SNR. We bin subcarriers to collect sufficient samples for an accurate estimate of SNR versus frequency. In Fig. 8 we present the SNR for three values of accumulated dispersion. The gray dotted line is theoretical fading. Each plot reports both 4R results in purple curves and 2R in green curves.

Consider the case of 32 GHz bandwidth OFDM with QPSK modulation. For 680 ps/nm accumulated dispersion, we see in Fig. 8a that 2R SNR has strong SNR dips, and the occurrence of these dips is similar to the theoretical fading pattern. For the 4R modulator, the SNR sees less oscillation over in-band frequency. With less dispersion, there are fewer oscillations in theoretical fading, as seen in Fig. 8b for 90 ps/nm accumulated dispersion. Again, we see good correlation between the 2R SNR degradation and the fading null. We conclude that energy leakage from the main signal band is contributing chromatic dispersion-induced fading for the 2R modulator.

We next examine the case of 48 GHz bandwidth OFDM with QPSK modulation. For 48 ps/nm accumulated dispersion, we see in Fig. 8c that the theoretical fading is similar to that Fig. 8b, i.e. a single fade. We see more clearly here that the 4R modulator also experiences fading effects, but to a much smaller degree than the 2R modulator. For this reason, we refer to the 4R modulator as being low chirp. Deeper fading is seen in the 48 GHz bandwidth signal, indicating stronger out-of-band power at higher frequency component due to chirp.

This article has been accepted for publication in IEEE/OSA Journal of Lightwave Technology. This is the author's version which has not been fully edited and content may change prior to final publication. Citation information: DOI 10.1109/JLT.2024.3362248

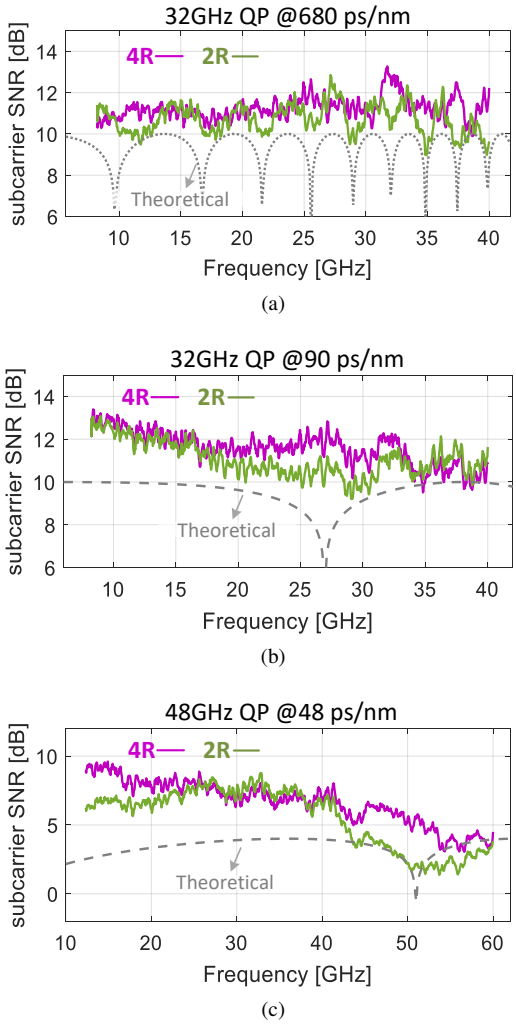

Fig. 8. Subcarrier SNR from 4R and 2R modulation: (a) 32-GHz QPSK with 680 ps/nm dispersion; (b) 32-GHz QPSK with 90 ps/nm dispersion; (c) 48-GHz QPSK with 48 ps/nm dispersion. Theoretical fading curves are plotted in gray dashed lines.

B. Performance improvement with 4R modulator

To quantify the performance improvement for reduced chirp, we compare the average SNR across subcarriers for each modulator. For the 4R modulator, $\mathrm{SNR}_{4R}(i)$ is estimated from recovered QAM constellation. To improve the quality of our estimates with an increased number of symbols, we combined two subcarriers into a single frequency bin of about 31.3 MHz (for 32 GHz signal) or 46.9 MHz (for 48 GHz signal). Similar values were used for the 2R modulator.

We define the low-chirp gain as

$$G = \frac{1}{N}\sum_{i=1}^{N}\mathrm{SNR}_{4R}(i) - \frac{1}{N}\sum_{i=1}^{N}\mathrm{SNR}_{2R}(i) \qquad (6)$$

with the calculation in linear scale and N =1024. Figure 9a plots the low-chirp gain in dB vs. accumulated dispersion. The x-axis has units of ps/nm, but we also include dashed vertical lines with the equivalent fiber length assuming standard single mode fiber (SMF) with dispersion coefficient D = 16.7 ps/nm/km at 1550 nm wavelength.

We examine three scenarios. We report results for QPSK signaling in solid lines for 32 GHz (square markers) and 48 GHz (triangle markers) OFDM bandwidth. For the case of 32 GHz OFDM bandwidth, we have sufficient SNR to also examine 16QAM modulation, with results plotted with circle markers.

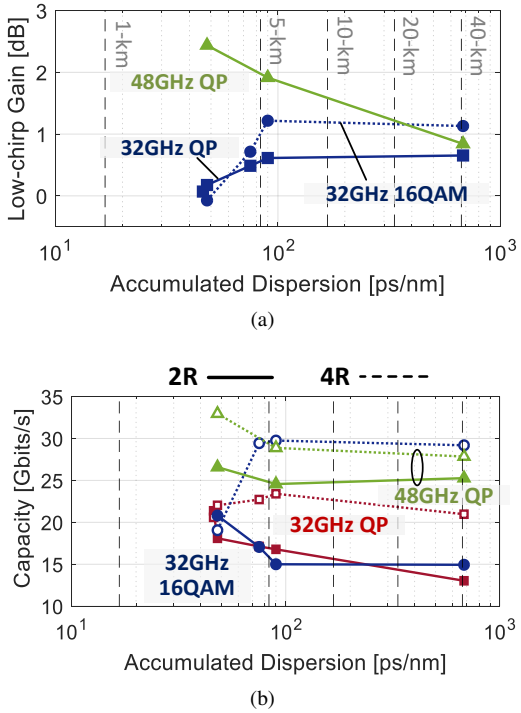

Fig. 9. Performance improvement by 4R modulation: (a) SNR gain versus accumulated dispersion (equivalent standard SMF distance for dispersion coefficient 16.7 ps/nm/km given in vertical lines); and (b) data capacity post-FEC.

For 32 GHz bandwidth signaling, SNR gain is very limited at low dispersion, with almost no gain at the lowest value of 48 ps/nm. The SNR gain is positive for other dispersion levels examined, at both modulation formats and at both OFDM bandwidths. Comparing modulation formats for 32 GHz OFDM bandwidth, we see peak gain of 0.6 dB for QPSK and 1.1 dB gain for 16QAM. This is not surprising, given the greater sensitivity of 16QAM to SNR degradation.

Higher gain is recorded with 48 GHz as fading is more severe at high frequencies; hence avoiding the fading with low-chirp operation is more critical. Note that for a fixed power budget, the 48 GHz has lower overall SNR, hence the fading effects also become more crippling. As component bandwidth increases, and systems push to higher baud rates and higher-order modulation, the chirp effect becomes more critical.

Finally, we consider the impact of chirp-induced fading on system throughput. The BER performance is not linear in SNR, hence gain in average SNR in (6) does not give complete picture. When SNR degrades below the forward error correction (FEC) threshold, the data on a subcarrier is lost and throughput is reduced. We set a threshold of 10.91 dB SNR with KP4 FEC [27] for 32 GHz QPSK, a threshold of 10.82 dB SNR with a 24% soft decision (SD)-FEC for 32 GHz

This article has been accepted for publication in IEEE/OSA Journal of Lightwave Technology. This is the author's version which has not been fully edited and content may change prior to final publication. Citation information: DOI 10.1109/JLT.2024.3362248

16QAM, and a threshold of 5.92 dB SNR with a 20% SD-FEC for 48 GHz QPSK.

We identify the valid subcarriers (with SNR above the FEC threshold) in each OFDM symbol for 2R and 4R modulators for the three cases and at each accumulated dispersion. From this we report the total throughput in Fig. 9b, which gives us another perspective on the improvement by the low-chirp. For QPSK format, 4R gives around around 41% improvement with 32 GHz bandwidth and 20% improvement at 90 ps/nm dispersion with 48 GHz bandwidth. This improvement can be exploited for greater margin or greater throughput. The greatest improvement is seen at high-order modulation. We nearly double the capacity in 32 GHz OFDM band with 16QAM at 90 ps/nm. Clearly, low-chirp modulation is of great benefit for high-order modulation.

V. Low-Chirp Improvement vis-à-vis SSBI

We quantify experimentally the performance improvement when using a 4R modulator. We confirm that 2R experiences higher levels of signal-to-signal beat interference (SSBI) than the 4R modulator. We present relative performance for various levels of accumulated dispersion.

A. Experimental confirmation of chirp-induced SSBI effect

The signal deterioration due to fading, even for the low-chirp case, dominates the SSBI effect. To confirm the performance degradation due to chirp-enhanced SSBI, we must eliminate the fading effect. To this end, we filter out the residual sideband.

As mentioned in Section II, we use the programmable optical filter (Waveshaper) to remove the lower sideband located at shorter wavelengths. We set the optical filter to have a flat response centered at around 1550.7 nm with 0.85 nm bandwidth. We captured the spectrum on a high resolution OSA with 0.16 pm resolution. The filtered optical spectrum is shown Fig. 10 for the two cases examined: 32 and 48 GHz OFDM bandwidth. We obtained 10 dB suppression on the unwanted sideband.

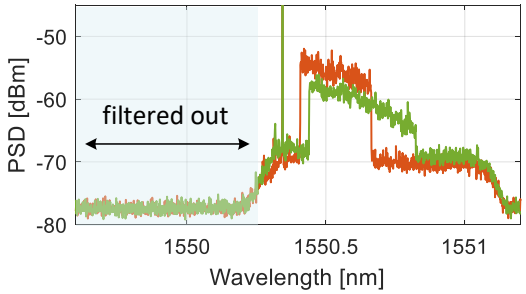

Fig. 10. Experimental optical spectrum with sideband filtering for 32 GHz and 48 GHz OFDM bandwidth.

Here we confirm there are no visible fading effects; in the next subsection we examine SSBI. We repeat the QPSK data transmission for 32 GHz and 48 GHz OFDM signals, now with filtered sidebands. We again estimate the SNR per subcarrier for the 4R and 2R modulators, reporting the results in Fig. 11 for 90 ps/nm of accumulated dispersion. We include the theoretical fading curve in gray for comparison. Comparing SNR with that in Fig. 8b, we see the SNR for the 32 GHz OFDM band is much flatter for both 2R and 4R modulators. In particular, the >2 dB dip reached at 30 GHz for the 2R modulator is no longer present. Hence, we have another indication that this dip was caused by the presence of the residual sideband.

B. Performance improvement with 4R modulator

In the simulations reported in Fig. 7, the highest frequencies see no SSBI with zero chirp (solid blue line), and SNR is flat. In the presence of chirp, the SNR at the highest frequencies sees the greatest signal degradation as the chirp increases. Consider in Fig. 11 the case with a 32 GHz OFDM bandwidth starting at 8 GHz. The SNR from 2R and 4R modulators is similar until 32 GHz. From this point, the 4R is visibly better, as highlighted in the box labeled "Enhanced SSBI".

The improved SSBI with 4R modulation is even more pronounced for the 48 GHz OFDM bandwidth. There is significant degradation at high frequencies, where we see the space between 4R and 2R modulators becoming larger in Fig. 8b. This demonstration supports our interpretation of the low-chirp advantage resulting from reduced enhancement of SSBI. The 4R modulator SNR is always better than that of the 2R modulator.

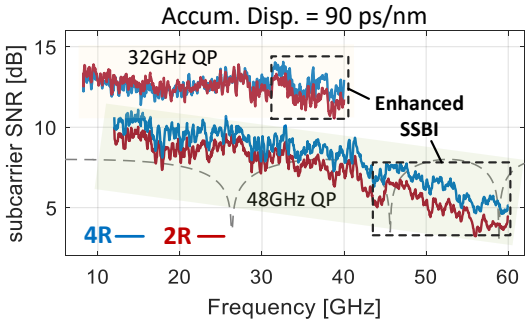

Fig. 11. Subcarrier SNR of 32 GHz and 48 GHz bandwidth signal with sideband filtering.

VI. Discussion

Accuracy of chirp model: In section III-B, we used a simple tanh to model the chirp effect in time series. The hyperbolic tangent function does not exactly follow the phase response seen in the experimental data in later sections. The model was, however, sufficient to capture the form and severity of signal distortion from chirp and from chirp imbalance. Since the experimental results support the trends predicted in our simulation model, we believe the model is sufficiently accurate for this purpose. Although we only consider static chirp, an MRM can also suffer from frequency-dependent chirp [28].

Chirp in push-pull configuration: In an ideal system, a push-pull configuration will cancel the chirp completely and achieve zero chirp. However, limitations in device technology and fabrication platforms make this impossible. Furthermore, the nonlinear response of the MRM in the high optical power

This article has been accepted for publication in IEEE/OSA Journal of Lightwave Technology. This is the author's version which has not been fully edited and content may change prior to final publication. Citation information: DOI 10.1109/JLT.2024.3362248

regime leads to asymmetric power response, as well as phase response, within the push-pull ring pair [29], [30]. While our experiments confirm that our 4R modulator suffered from observable chirp-induced effects, these effects were much attenuated. Even within device limitations, our 4R modulator offers a significant reduction in effective chirp that is critical for SSB-OFDM systems.

Influence of filtered residual sideband on SSBI: We attribute the improved 4R modulator SNR in Fig. 11 to reducing the chirp-enhanced SSBI. Although our filtering eliminated fading, it did not eliminate the disparity in OFDM signal power for 2R and 4R modulators. As 2R modulation leaks more power from the desired signal, that causes a greater SNR penalty in-band, which could also explain the improvement with 4R.

We believe the impact of in-band power discrepancy between 2R and 4R cases is not dominant. We could not observe this difference on the optical spectrum analyzer. As a final test, we repeated transmission at various levels of accumulated dispersion and recorded the low-chirp gain for the SSBI scenario in Fig. 12. We see that for both 32 GHz QPSK and 16QAM, the low-chirp gain has little correlation with dispersion, reinforcing our interpretation. At 48 GHz there is significantly more gain compared to the 32 GHz OFDM signal, as we expected since the SSBI is more severe at high frequencies.

At greater accumulated dispersion, the 48 GHz QPSK signal sees less gain with the 4R configuration. We attribute this decrease to the interplay of the residual chirp with an increasing number of in-band notches. A similar trend is seen with 32 GHz. The slope of the decrease may be less for 32 GHz as it sees fewer notches with the smaller passband.

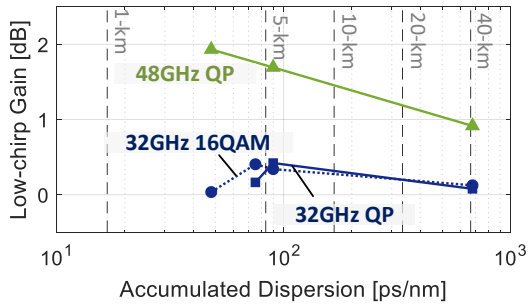

Fig. 12. Low-chirp gain with sideband filtering vs. accumulated dispersion.

MRM versus MZM: An MZM with push-pull configuration can also achieve zero-chirp modulation and perhaps better performance. Both MZM and MRM could be optimized for specific applications. For example, MZM phase shifter length will impact bandwidth and efficiency; the static power transfer function of an MRM could be designed to align with desired laser wavelength to reduce thermal control. While the MZM is less sensitive to variations in power and temperature, our focus on MRM for OFDM and direct-detection in RAN or PON applications is based on advantages of low power consumption and wavelength selectivity.

VII. Conclusion

We demonstrate a performance improvement for SSB OFDM when using a 4R, low-chirp modulation via a push-pull SiP MRM. We have isolated two sources of chirp degradation: chirp-induced residual sideband and chirp-enhanced SSBI. We validate these two sources of degradation via simulation and experiments. We use a simple chirp model to capture the chirp impairments in simulation. The impact of chirp-induced residual sideband varies with the accumulated dispersion. In our experimental study we quantify the low-chirp gain as reaching 0.6 dB for 16QAM with a 32 GHz OFDM bandwidth, and 2.4 dB for QPSK with 48 GHz OFDM bandwidth. We were able to examine the enhanced SSBI by filtering out the unwanted sideband. Low-chirp modulation is clearly effective in improving the transmission performance of the OFDM subcarrier with high frequency.

Acknowledgment

The authors acknowledge research funding from NSERC Canada (CRDPJ528381) and a fabrication subsidy from CMC Microsystems. We also thank our technician Simon Levasseur for packaging and technical support.

Appendix A
Spectral Effect of Fading

Consider DSB modulation with a real signal $s_0(t)$, its spectrum $S_0(f)$ has conjugate symmetry

$$S_0^*(f) = S_0(-f). \tag{7}$$

The transfer function of chromatic dispersion is

$$H_{CD}(f) = \exp\left[j\,\frac{\beta_2}{2}(2\pi f)^2\, z\right] \tag{8}$$

where β_2 is group velocity dispersion (GVD) of the fiber, and z is propagation distance. To simplify notation, we designate phase shift φ_f at frequency f

$$\varphi_f = \frac{\beta_2}{2}(2\pi f)^2\, z, \tag{9}$$

an even function of f. With modulation at the quadrature point and fiber transmission, the signal spectrum becomes

$$S(f) = S_c + S_0(f)\exp(j\varphi_f) \tag{10}$$

where S_c represents the carrier in frequency domain, with constant power S_c^2. For direct detection the signal spectrum after photodetection is

$$R(f) = |S(f)|^2 = S_c^2 + S_c(S(f) + S^*(f)) + S(f)\cdot S^*(f). \tag{11}$$

Given that the optical carrier has much greater power than the signal $S(f)$, we neglect the last term in (11). The DC component S_c^2 is filtered at the receiver. Therefore the RF spectrum is

$$\begin{aligned} R_{RF}(f) &= S_c\left[S_0(f)\exp(j\varphi_f) + S_0^*(f)\exp(j\varphi_f)^*\right] \\ &= S_c\left[S_0(f)\exp(j\varphi_f) + S_0(-f)\exp(j\varphi_f)\right] \\ &= 2S_cS_0(f)\cos(j\varphi_f) \end{aligned} \tag{12}$$

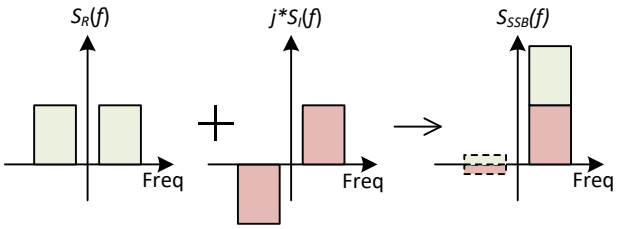

Fig. 13. Spectrum of IQ components of SSB signal and two possible situations of residual sideband.

To create a SSB signal, we force the IQ components to have Hermitian symmetry. A residual sideband will form if there is unbalanced chirp, as we simulated in Section III-C. This is illustrated in Fig. 13. There are two possible phase relationships between the two sidebands due to imperfect cancellation

$$S^*_{res}(f) = \gamma S_{main}(-f). \tag{13}$$

or

$$S^*_{res}(f) = -\gamma S_{main}(-f). \tag{14}$$

Let γ be the power ratio of residual sideband to main sideband. Then we can derive the received electrical spectrum based on Eq. (10)-(12):

$$R(f) = 2(1-\gamma)S_c S(f) + 2\gamma S_c S(f)\cos\varphi_f \tag{15}$$

or

$$R(f) = 2(1-\gamma)S_c S(f) + 2\gamma S_c S(f)\sin\varphi_f \tag{16}$$

Here $S(f)$ represents main sideband of SSB signal. The second term is the impact of fading. The fading pattern can be either (15) or (16). For the theoretical fading in Fig. 8, we plot the spectrum consistent with our measurements. We provide a captured electrical spectrum from 2R modulation in Fig. 14 to illustrate the fading issue from raw data.

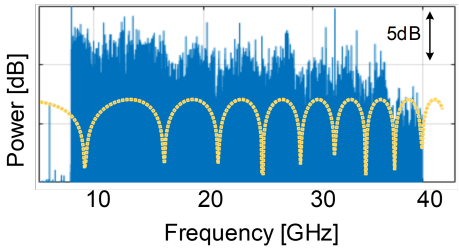

Fig. 14. Example of received electrical spectrum from 2R modulation with 32 GHz signal bandwidth and 680 ps/nm dispersion. Theoretical fading curve is given in yellow dotted line.

Appendix B
Tuning and Stabilization

We have MZIs equipped with thermal heaters to allow us to tune power splits. These are located before the spilt of I/Q branches and split of push-pull rings. We have on-chip Ge-on-silicon photodetectors to monitor the power from drop port of the rings. We tune the voltage to the heaters and monitor the power from the ring. We carefully adjust voltages to balance the power on all four rings.

To control thermal runoff, we designed an in-house initialization program for all heaters controlling power balance, resonance wavelength and operating point. The initialization provides only coarse thermal stabilization. We then tweak the RF voltage, to gradually tune the heater to optimize SSB signal modulation. We monitor the power from drop ports when we finalize tuning to ensure the measurement is repeatable.

References

[1] P. T. Dat, A. Kanno, N. Yamamoto, and T. Kawanishi, "Seamless convergence of fiber and wireless systems for 5G and beyond networks," *J. Lightwave Technol.*, vol. 37, no. 2, pp. 592–605, 2018.

[2] M. Asghari and A. V. Krishnamoorthy, "Energy-efficient communication," *Nat. Photon.*, vol. 5, no. 5, pp. 268–270, 2011.

[3] A. J. Lowery and J. Armstrong, "Orthogonal-frequency-division multiplexing for dispersion compensation of long-haul optical systems," *Opt. Express*, vol. 14, no. 6, pp. 2079–2084, 2006.

[4] C. Lim, A. Nirmalathas, M. Bakaul, K.-L. Lee, D. Novak, and R. Waterhouse, "Mitigation strategy for transmission impairments in millimeter-wave radio-over-fiber networks," *J. Opt. Netw.*, vol. 8, no. 2, pp. 201–214, 2009.

[5] J. Maeda, T. Katoh, and S. Ebisawa, "Effect of Fiber Dispersion on Subcarrier QAM Signal in Radio-Over-Fiber Transmission," *J. Lightwave Technol.*, vol. 30, no. 16, pp. 2625–2632, 2012.

[6] D. F. Hewitt, "Orthogonal frequency division multiplexing using baseband optical single sideband for simpler adaptive dispersion compensation," in *Conference on Optical Fiber Communication*, 2007, pp. 1–3.

[7] Y. Tong, C.-W. Chow, G.-H. Chen, C.-W. Peng, C.-H. Yeh, and H. K. Tsang, "Integrated silicon photonics remote radio frontend (RRF) for single-sideband (SSB) millimeter-wave radio-over-fiber (ROF) systems," *IEEE Photonics Journal*, vol. 11, no. 2, pp. 1–8, 2019.

[8] C. Y. Wong, S. Zhang, Y. Fang, L. Liu, T. Wang, Q. Zhang, S. Deng, G. N. Liu, and X. Xu, "Silicon IQ modulator for next-generation metro network," *J. Lightwave Technol.*, vol. 34, no. 2, pp. 730–736, 2015.

[9] B.-M. Yu, J.-M. Lee, C. Mai, S. Lischke, L. Zimmermann, and W.-Y. Choi, "Single-chip Si optical single-sideband modulator," *Photon. Research*, vol. 6, no. 1, pp. 6–11, 2018.

[10] M. Lyu, Y. Xu, L. A. Rusch, and W. Shi, "Single-sideband OFDM transmission via a silicon microring IQ modulator," *IEEE Photon. Technol. Lett.*, vol. 31, no. 2, pp. 145–148, 2018.

[11] L. Zhang, J.-Y. Yang, M. Song, Y. Li, B. Zhang, R. G. Beausoleil, and A. E. Willner, "Microring-based modulation and demodulation of DPSK signal," *Opt. Express*, vol. 15, no. 18, pp. 11 564–11 569, 2007.

[12] Koyama, F. and Iga, K., "Frequency chirping in external modulators," *J. Lightwave Technol.*, vol. 6, no. 1, pp. 87–93, 1988.

[13] D. J. Thomson, F. Y. Gardes, S. Liu, H. Porte, L. Zimmermann, J.-M. Fedeli, Y. Hu, M. Nedeljkovic, X. Yang, P. Petropoulos *et al.*, "High performance Mach–Zehnder-based silicon optical modulators," *IEEE Journal of Selected Topics in Quantum Electronics*, vol. 19, no. 6, pp. 85–94, 2013.

[14] Zhang, Lin and Li, Yunchu and Yang, Jeng-Yuan and Song, Muping and Beausoleil, Raymond G. and Willner, Alan E., "Silicon-Based Microring Resonator Modulators for Intensity Modulation," *J. Selec. Topics Quantum Electron.*, vol. 16, no. 1, pp. 149–158, 2010.

[15] Wang, Zhao and Gao, Yuliang and Kashi, Aazar S. and Cartledge, John C. and Knights, Andrew P., "Silicon Microring Modulator for Dispersion Uncompensated Transmission Applications," *J. Lightwave Technol.*, vol. 34, no. 16, pp. 3675–3681, 2016.

[16] David W. U Chan, Xiong Wu, Zunyue Zhang, Chao Lu, Alan Pak Tao Lau, and Hon Ki Tsang, "C-band 67 GHz silicon photonic microring modulator for dispersion-uncompensated 100 Gbaud PAM-4," *Opt. Lett.*, vol. 47, no. 11, pp. 2935–2938, 2022.

[17] D. Patel, V. K. Singh, and U. Dalal, "Performance analysis of optical double sideband and optical single sideband generation using mach zehnder modulator chirp and extinction ratio over different fiber link," in *2017 2nd International Conference for Convergence in Technology (I2CT)*, 2017, pp. 721–726.

[18] W.-R. Peng, X. Wu, V. R. Arbab, B. Shamee, L. C. Christen, J.-Y. Yang, K.-M. Feng, A. E. Willner, and S. Chi, "Experimental demonstration of a coherently modulated and directly detected optical OFDM system using an RF-tone insertion," in *Conference on Optical Fiber Communication*, 2008, pp. 1–3.

[19] C.-C. Wei, "Small-signal analysis of oofdm signal transmission with directly modulated laser and direct detection," *Opt. Lett.*, vol. 36, no. 2, pp. 151–153, Jan 2011.
[20] N. S. André, K. Habel, H. Louchet, and A. Richter, "Adaptive nonlinear volterra equalizer for mitigation of chirp-induced distortions in cost effective imdd ofdm systems," *Opt. Express*, vol. 21, no. 22, pp. 26 527–26 532, 2013.
[21] C.-M. Chang, P. Dong, C. Gui, and G. de Valicourt, "Low-chirp push-pull microring modulators," in *Conference on Optical Fiber Communication*. Optica Publishing Group, 2016, pp. Th4H–2.
[22] C.-M. Chang, G. de Valicourt, S. Chandrasekhar, and P. Dong, "Differential Microring Modulators for Intensity and Phase Modulation: Theory and Experiments," *J. Lightwave Technol.*, vol. 35, no. 15, pp. 3116–3124, 2017.
[23] A. Geravand, Z. Zheng, S. Levasseur, L. A. Rusch, and W. Shi, "UltraCompact Silicon Modulator for 124 GBaud Coherent Optical Links," in *IEEE Silicon Photonics Conference (SiPhotonics)*, 2023.
[24] ——, "Ultra-Compact Silicon IQ Modulator Beyond 100 GBaud," in *European Conference on Optical Communications*, 2023, pp. M.A2–1.
[25] Z. Zheng, A. Geravand, S. Levasseur, L. A. Rusch, and W. Shi, "Silicon Microring Modulator Achieving 1 Tb/s Net Rate with Coherent Detection," in *European Conference on Optical Communications*, 2023, pp. Th.C2–6.
[26] M. J. Shawon and V. Saxena, "Optical Linearization of Silicon Photonic Ring-Assisted Mach-Zehnder Modulator," *arXiv*, no. 2308.15763, 2023.
[27] S. Bhoja, V. Parthasarathy, and Z. Wang, "FEC Codes for 400 Gbps 802.3bs," [Online]. Available: https://www.ieee802.org/3/bs/public/14_11/parthasarathy_3bs_01a_1114.pdf.
[28] E. Weckenmann, L. Bramerie, M. Gay, D. Pérez-Galacho, F. Boeuf, L. Deniel, D. Marris-Morini, and C. Peucheret, "Frequency Chirp Characterization of Silicon Ring Resonator Modulators," *IEEE Photon. Technol. Lett.*, vol. 34, no. 12, pp. 653–656, 2022.
[29] C. Sun, M. Wade, M. Georgas, S. Lin, L. Alloatti, B. Moss, R. Kumar, A. H. Atabaki, F. Pavanello, J. M. Shainline, J. S. Orcutt, R. J. Ram, M. Popović, and V. Stojanović, "A 45 nm CMOS-SOI Monolithic Photonics Platform With Bit-Statistics-Based Resonant Microring Thermal Tuning," *IEEE J. Solid-State Circuits*, vol. 51, no. 4, pp. 893–907, 2016.
[30] M. de Cea, A. H. Atabaki, and R. J. Ram, "Power handling of silicon microring modulators," *Opt. Express*, vol. 27, no. 17, pp. 24 274–24 285, 2019.